

An *ab initio* potential energy surface for Ne–CO

George C. McBane

Department of Chemistry, The Ohio State University, Columbus, Ohio 43210

Slawomir M. Cybulski

Department of Chemistry and Biochemistry, Miami University, Oxford, Ohio 45056

(Received 1 February 1999; accepted 30 March 1999)

A new *ab initio* two-dimensional potential energy surface for the Ne–CO interaction is described. The surface was obtained by the supermolecule method at the CCSD(T) level of theory. It is compared with several experimental data sets and with the symmetry-adapted perturbation theory (SAPT) surface of Moszynski *et al.* [J. Phys. Chem. A **101**, 4690 (1997)]. The new surface gives modestly better predictions of experimental results that depend on close approach of Ne to CO, but does not describe the ground state geometry as well as the SAPT surface. © 1999 American Institute of Physics. [S0021-9606(99)00924-1]

I. INTRODUCTION

The first *ab initio* potential energy surface for the rigid rotor CO–Ne interaction was published by Moszynski *et al.* in 1997.¹ Their surface, obtained with symmetry-adapted perturbation theory (SAPT), agreed well with the infrared absorption spectra of NeCO² and bulk property data for Ne–CO mixtures^{3–5} available at the time. Since 1997 the SAPT surface has also been compared with more extensive infrared results.⁶ Its predictions were still useful, although the agreement with IR spectra of vibrationally excited complexes was not as good as that for the ground state.

Moszynski *et al.* also reported an empirically modified version of their surface. They chose small empirical scalings to improve the agreement with a few rotational lines in the NeCO infrared spectrum. Since they did not construct a separate surface with $v_{\text{CO}}=1$, the scaling parameters served two purposes: to slightly modify the shape of the *ab initio* ground state surface, and to allow for changes in the surface shape upon vibrational excitation of the CO. With two scaling parameters they were able to improve agreement with many infrared lines by as much as an order of magnitude.

New measurements of state-to-state integral cross sections for rotational excitation of CO by Ne are reported in the accompanying experimental paper.⁷ Those are the first experimental data that are very sensitive to anisotropy in the repulsive wall of the Ne–CO potential. Cross sections calculated from the SAPT surface reproduced the overall rotational contour well, but did not accurately reproduce the interference oscillations that appear at low Δj . Since it is relatively difficult to evaluate the short range repulsion energies accurately in a perturbation theory calculation, it seemed plausible that the SAPT surface might be less accurate in the repulsive region than at larger Ne–CO separations, and that some improvements in the description of the repulsive interactions might be possible.

In this paper we report two new Ne–CO surfaces, obtained with supermolecule rather than perturbation theory techniques. A discussion of advantages and disadvantages of, and the relationship between, the supermolecule and pertur-

bation theory approaches can be found in the recent review article by Chałasiński and Szczęśniak.⁸ The *ab initio* calculations were performed at the CCSD(T) level of theory with large basis sets, and represent the current state of the art for supermolecule calculations on a system of this size.^{9,10} In the remainder of this paper we describe the construction of the new surfaces, compare their predictions and those of the SAPT surface with experimental data, and discuss the differences. Since our intent is to compare the two *ab initio* approaches, most of the comparisons are made with the *ab initio* SAPT surface and not with its empirically modified variant.

II. CONSTRUCTION OF SURFACES

A. Electronic structure calculations

The potential energy surfaces for the Ne–CO complex were calculated using the supermolecule single and double excitation coupled-cluster theory with noniterative perturbational treatment of triple excitations [CCSD(T)].¹¹ The calculations used the augmented correlation-consistent triple zeta (aug-cc-pVTZ) basis set^{12–14} with an additional set of bond functions. Two sets of bond functions were used: the (3s3p2d) set of Tao and Pan¹⁵ as well as a larger (3s3p2d1f1g) set used by Koch *et al.*¹⁶ The overall basis sets will be denoted by aug-cc-pVTZ+(3s3p2d) and aug-cc-pVTZ+(3s3p2d1f1g) and the corresponding surfaces by S1 and S2, respectively. In all calculations the CO bond was fixed at the experimental value of 1.128 Å. The counterpoise procedure of Boys and Bernardi¹⁷ was used to correct for basis set superposition error (BSSE.) CCSD(T) calculations were performed with the efficient program^{18,19} available in the MOLPRO 96 package.²⁰

The CCSD(T) interaction energies obtained with the larger basis set are given in Table I. R signifies the distance from the Ne atom to the center of mass of ¹²C¹⁶O, and Θ gives the angle between the vector from the CO center of mass to the Ne atom and the vector pointing from the CO center of mass to the O atom. $\Theta=0$ therefore represents the

TABLE I. The CCSD(T) interaction energies (in μE_h) obtained with the aug-cc-pVTZ+(3s3p2d1f1g) basis set. Interaction energies for geometries in the vicinity of the minimum: $\Theta=75^\circ$: (-219.7, $R=3.35 \text{ \AA}$), (-219.9, $R=3.40 \text{ \AA}$), (-217.4, $R=3.45 \text{ \AA}$); $\Theta=80^\circ$: (-220.7, $R=3.35 \text{ \AA}$), (-220.6, $R=3.40 \text{ \AA}$), (-217.4, $R=3.45 \text{ \AA}$); $\Theta=85^\circ$: (-219.9, $R=3.35 \text{ \AA}$), (-219.9, $R=3.40 \text{ \AA}$), (-216.9, $R=3.45 \text{ \AA}$).

R	$\Theta=0^\circ$	20	40	60	80	100	120	140	160	180
2.25	11 809.5	12 803.5
2.50	.	.	10 351.9	5675.2	3706.0	4390.6	9868.3	.	.	.
2.75	6136.7	5078.9	3019.4	1502.7	896.5	1241.0	3556.9	10 147.1	.	.
3.00	1590.8	1262.4	629.9	179.7	14.1	157.2	1059.7	3702.0	7997.3	10 419.8
3.25	199.9	108.4	-60.7	-169.4	-203.5	-157.0	155.7	1143.5	2780.6	3700.6
3.50	-156.8	-175.1	-203.8	-213.8	-213.1	-206.3	-122.0	207.0	787.9	1119.3
3.75	-201.1	-199.7	-191.6	-178.2	-171.3	-177.5	-172.8	-89.4	89.3	197.0
4.00	-167.0	-161.6	-147.6	-132.5	-126.4	-135.3	-152.9	-152.0	-116.0	-89.9
4.25	-122.6	-118.0	-106.4	-94.6	-90.3	-98.6	-118.5	-139.3	-148.2	-148.8
4.50	-86.5	-83.3	-75.2	-67.0	-64.2	-70.8	-87.4	-109.3	-127.8	-135.0
5.00	-43.0	-41.7	-38.1	-34.4	-33.2	-36.8	-45.9	-58.9	-71.4	-76.5
6.00	-12.3	-12.1	-11.3	-10.6	-10.5	-11.5	-13.6	-16.5	-19.2	-20.0
7.00	-4.3	-4.3	-4.1	-3.9	-3.9	-4.2	-4.8	-5.6	-6.2	-6.5

linear Ne–O–C geometry. The bond functions were placed in the middle of the R vector.

In addition to the values presented in the table, a few additional calculations were performed in the vicinity of the minimum which occurs at approximately $R=3.4 \text{ \AA}$ and $\Theta=80^\circ$. At this geometry the aug-cc-pVTZ+(3s3p2d) basis gives an interaction energy of $-214.2 \mu E_h$. The aug-cc-pVTZ+(3s3p2d1f1g) basis set gives at the same geometry $-220.6 \mu E_h$. Calculations with the smaller aug-cc-pVDZ+(3s3p2d) and the larger aug-cc-pVQZ+(3s3p2d) basis sets give CCSD(T) interaction energies of $-202.3 \mu E_h$ and $-220.0 \mu E_h$, respectively. All the results clearly indicate that the interaction becomes stronger as basis set size is increased and it thus appears that because of the basis set incompleteness the depth of the potentials developed in this work is slightly underestimated.

Interestingly, the MP4 method yields an interaction energy of $-224.7 \mu E_h$ when the aug-cc-pVTZ+(3s3p2d) basis set is used and $-231.3 \mu E_h$ with aug-cc-pVTZ+(3s3p2d1f1g).

B. Fitting procedure

The *ab initio* points were fitted to a two-dimensional model potential proposed by Bukowski *et al.*²¹ and used by other researchers.^{22,23} The function contains short range $V_{\text{sh}}(R, \Theta)$ and asymptotic $V_{\text{as}}(R, \Theta)$ contributions:

$$V(R, \Theta) = V_{\text{sh}}(R, \Theta) + V_{\text{as}}(R, \Theta). \quad (1)$$

The short range potential consisted of the exponential function

$$V(R, \Theta) = G(R, \Theta) e^{D(\Theta) - B(\Theta)R}, \quad (2)$$

where $D(\Theta)$, $B(\Theta)$, and $G(R, \Theta)$ were all expansions in Legendre polynomials, $P_l^0(\cos \Theta)$. Their explicit forms were

$$X(\Theta) = \sum_{l=0}^L x^l P_l^0(\cos \Theta) \quad (3)$$

for $D(\Theta)$ and $B(\Theta)$ ($X=D$ or B) and

$$G(R, \Theta) = \sum_{l=0}^L (g_0^l + g_1^l R + g_2^l R^2 + g_3^l R^3) P_l^0(\cos \Theta). \quad (4)$$

All expansions were truncated at $l=5$.

The asymptotic part included a damped-dispersion expansion, which was truncated at the R^{-7} term, i.e., $n_{\text{max}}=7$,

$$V_{\text{as}}(R, \Theta) = \sum_{n=6}^{n_{\text{max}}} \sum_{l=0,2,\dots \text{ or } l=1,3,\dots}^{n-4} f_n(B(\Theta)R) \frac{C_n^l}{R^n} P_l^0(\cos \Theta) \quad (5)$$

and which included the Tang–Toennies damping function²⁴ (f_n)

$$f_n(x) = 1 - e^{-x} \sum_{k=0}^n \frac{x^k}{k!} \quad (6)$$

and dispersion coefficients (C_n^l) obtained from a least squares fit. The rms error of the fit was $0.50 \mu E_h$ for the S1 surface and $0.65 \mu E_h$ for the S2 surface. The maximum absolute error of the fit did not exceed $1.8 \mu E_h$ and $2.0 \mu E_h$ for the S1 and S2 surfaces, respectively. Table II lists the fit coefficients for S2. Tables of energies and fit coefficients for S1, and a Fortran subroutine to evaluate the fitted energies for both surfaces as functions of position, are available as supplementary material.

C. Features of the surfaces

The minimum on S1, with energy $-214.3 \mu E_h$, is at $R=3.394 \text{ \AA}$ and $\Theta=79.76^\circ$; that on S2 is a $R=3.385 \text{ \AA}$ and $\Theta=80.15^\circ$ and has energy $-221.0 \mu E_h$. Figure 1 shows potential energy curves at five different values of Θ for S2 and the SAPT surface of Moszynski *et al.*¹ The well on S2 is slightly shallower and less anisotropic than that on the SAPT surface. The low energy repulsive wall on S2 is also less anisotropic than that of the SAPT surface.

Figure 2 shows a contour map of S2 in the attractive region; the figure is comparable to Fig. 3(a) in Ref. 1. Potential contours in the repulsive region for the SAPT and S2

TABLE II. Fit coefficients for S2. $C_6^0 = -597.085\ 26$; $C_6^2 = -114.316\ 30$; $C_7^1 = -1206.647\ 64$; $C_7^3 = -258.362\ 09$.

	$l=0$	$l=1$	$l=2$	$l=3$	$l=4$	$l=5$
b	12.131 04	-0.124 89	-0.078 83	-0.007 78	0.387 97	-0.073 21
d	-3.148 22	-0.089 74	0.207 26	0.000 09	-0.124 26	0.023 04
g_0	0.408 25	-0.557 09	0.582 91	0.258 17	0.234 34	0.257 47
g_1	-0.056 58	0.746 44	-0.178 81	-0.067 44	-0.155 87	-0.202 70
g_2	-0.012 37	-0.214 46	0.029 74	0.010 09	0.043 04	0.054 13
g_3	0.000 46	0.017 02	-0.004 64	-0.001 82	-0.004 26	-0.004 74

surfaces are shown in the accompanying experimental paper.⁷ The repulsive walls are similar near the O end of the molecule. They are rather different near the T-shaped configuration; for example, at $R=2.54\text{ \AA}$ and $\Theta=90^\circ$, the SAPT and S2 energies respectively are 2734.3 and 3010.3 μE_h (600.10 and 660.68 cm^{-1}). The potential curves are similar again near $\Theta=150^\circ$, and at the C end the SAPT surface is more repulsive than S2. At 3.44 \AA in the Ne-C-O arrangement, the SAPT and S2 energies are 1920.7 and 1575.4 μE_h (421.54 and 345.77 cm^{-1}), respectively.

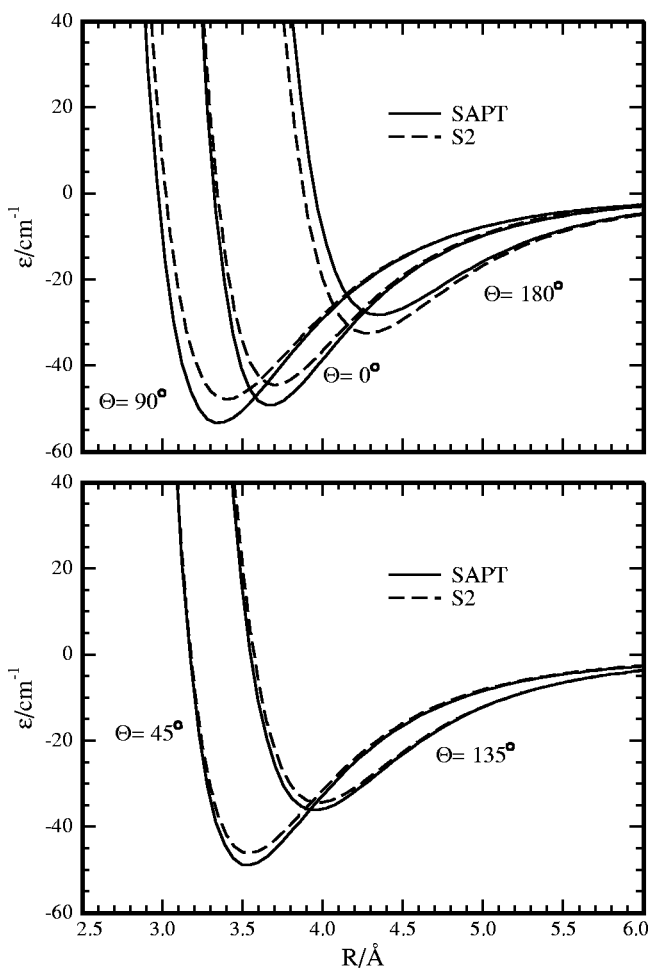


FIG. 1. Potential energy curves for the S2 and SAPT surfaces at several angles.

III. DYNAMICAL CALCULATIONS

A. Bound energy levels

The energies of bound states on S2 were determined by the coupled-channel approach with the BOUND program of Hutson.^{25,26} A rotational basis set including CO rotational levels up to $j=16$ and a convergence tolerance of 0.0002 cm^{-1} was used. The diabatic modified log-derivative method of Manolopoulos²⁷ was used for all calculations; results from step sizes of 0.03 and 0.06 \AA were extrapolated to zero step size to estimate the bound level energies. The reduced mass of the Ne-CO system ($11.663\ 21$ amu) and the rotational constant of CO ($1.922\ 516\ 5\text{ cm}^{-1}$) were the same values used by Moszynski *et al.*¹ The total numerical error in the energies, including that from basis set truncation and finite distance of propagation, probably does not exceed 0.001 cm^{-1} for levels with total angular momentum $J\leqslant 7$.

The ground state on S2 has an energy of -31.0995 cm^{-1} relative to separated Ne and CO. The average separation between Ne and the CO center of mass is $\langle R \rangle = 3.673\text{ \AA}$, with standard deviation $(\langle R^2 \rangle - \langle R \rangle^2)^{1/2} = 0.27\text{ \AA}$. The average bond angle $\langle \Theta \rangle = \cos^{-1}(\langle P_1(\cos \Theta) \rangle) = 66.56^\circ$. An indication of the angular extent of the ground state wave function is given by $\cos^{-1}[(2\langle P_2(\cos \Theta) \rangle + 1)/3]^{1/2}$, whose value is 56.03° . S2 has a Ne-CO bond longer by 0.037 \AA and a slightly more acute bond angle than the SAPT surface. On

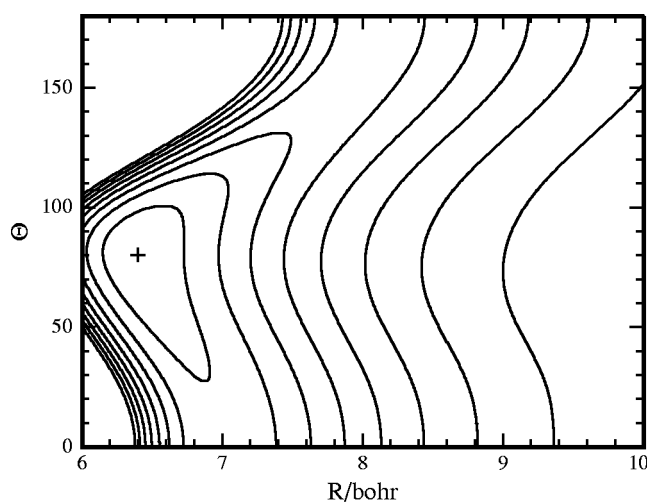


FIG. 2. Potential energy contours of S2 in the attractive region. The cross shows the position of the minimum, with energy -48.504 cm^{-1} . The lowest energy contour is at -45 cm^{-1} and the spacing is 5 cm^{-1} .

TABLE III. Observed and calculated microwave absorption spectra, in cm^{-1} . The level energies on S2 are (in cm^{-1}): $-31.0995 (0_{00})$, $-27.3425 (1_{11})$, $-27.3276 (1_{10})$.

Transition	Expt (Ref. 31)	SAPT (Ref. 1)	Δ	S2	Δ
$1_{01} \leftarrow 0_{00}$	0.217 41	0.218	-0.001	0.213	0.004
$2_{02} \leftarrow 1_{01}$	0.434 51	0.436	-0.001	0.427	0.007
$2_{12} \leftarrow 1_{11}$	0.416 65	0.420	-0.003	0.410	0.007
$2_{11} \leftarrow 1_{10}$	0.446 03	0.450	-0.004	0.440	0.006
$3_{03} \leftarrow 2_{02}$	0.650 98	0.652	-0.002	0.639	0.012
$3_{13} \leftarrow 2_{12}$	0.624 25	0.629	-0.005	0.615	0.013
$3_{12} \leftarrow 2_{11}$	0.668 30	0.675	-0.007	0.659	0.009
$4_{04} \leftarrow 3_{03}$	0.866 52	0.869	-0.002	0.851	0.016
$4_{14} \leftarrow 3_{13}$	0.830 96	0.839	-0.008	0.817	0.014

both surfaces the ground state wave function is fairly tightly localized in R but delocalized in Θ .

B. Scattering calculations

Integral and differential scattering cross sections and pressure broadening cross sections were computed with the MOLSCAT program of Hutson and Green.²⁸ Both coupled states (CS)²⁹ and close-coupled (CC) calculations were performed, as described below. The hybrid log-derivative/Airy propagator of Manolopolous and Alexander was used.³⁰ In every calculation all the open rotational channels and at least one closed channel were included in the rotational basis set. Partial wave sums were usually terminated when inelastic cross sections had converged to 0.02 \AA^2 and elastic cross sections to 1.0 \AA^2 .

IV. COMPARISON WITH EXPERIMENTS

A. Microwave spectra

Table III shows the wavenumbers of the nine microwave lines of $^{20}\text{Ne}-^{12}\text{C}^{16}\text{O}$ observed by Walker *et al.*,³¹ and the corresponding wavenumbers calculated from the *ab initio* SAPT potential and S2. Differences (experiment-theory) are also given.

Microwave frequencies computed from S2 are consistently lower than the observed ones. Frequencies from the SAPT surface are consistently higher, but the error is usually two to four times less. These differences are consistent with the slightly longer $\langle R \rangle$ computed from S2. The value of $\langle R \rangle$ estimated by Walker *et al.* from the C rotational constant, 3.675 \AA , agrees almost perfectly with the value computed from S2 and is slightly longer than that computed from the

SAPT surface. It is clear from the microwave frequencies themselves, though, that the SAPT surface gives a more accurate description of the geometry of the ground state.

The ground state on the empirically scaled SAPT surface has a slightly greater binding energy than that on the *ab initio* SAPT surface, and a value of $\langle R \rangle$ that is 0.012 \AA shorter. Its agreement with the microwave spectrum is not as good; the errors are similar in magnitude to those of S2 but in the opposite direction.

S1, computed with a smaller basis set, has a yet larger $\langle R \rangle$ and gives microwave frequency errors roughly another 25% greater than those of S2. The f and g bond functions added to the basis set in S2 deepened the well and reduced the value of $\langle R \rangle$, bringing S2 toward better agreement with experiment. The single-point calculations with yet larger basis sets described above suggest that further expansion of the basis set would further deepen the well and reduce the disagreement with the microwave data.

B. Infrared spectra

The richest source of information about the bound levels of Ne-CO is the infrared work of Randall *et al.*² and McKellar and Chan.⁶ The SAPT and S2 *ab initio* surfaces, however, were both computed with the bond length of CO fixed at its equilibrium value. Positions of IR lines can therefore not be computed directly from the surfaces. Moszynski *et al.* compared the SAPT surface with the IR data of Randall *et al.* with an empirical procedure, as described briefly earlier.

The more recent IR data of McKellar and Chan include many lines with $K=2$ or 3, and several hot bands with $v_2 = 1$ bending mode excitation. With these new data, they were able to fit molecular constants separately for the $v_{\text{CO}} = 0$ and $v_{\text{CO}} = 1$ van der Waals complexes. These constants provide us with a much more direct means of comparing experiment and theory: We can simply evaluate the energies of the bound levels of NeCO ($v_{\text{CO}}=0$) from the experimental constants and from the *ab initio* surfaces.

Tables IV and V show the differences between the energy levels calculated from the constants of McKellar and Chan⁶ and those calculated from the S2 and SAPT surfaces. Nearly all the observed lines in the IR spectrum are fit to within 0.001 cm^{-1} by the constants, so the “experimental” energies in these tables may be regarded as exact. The experiments do not provide the dissociation energy of the ground state, and that was set to zero.

TABLE IV. Errors (experimental-theoretical, in cm^{-1}) in the energies of bound levels for the vibrational ground state of Ne-CO.

J	$K=1,e$		$K=1,f$		$K=2,e$		$K=2,f$		$K=3,e$		$K=3,f$	
	SAPT	S2										
1	-0.183	-0.332	-0.184	-0.333								
2	-0.187	-0.326	-0.188	-0.326	-0.164	-0.490	-0.162	-0.489				
3	-0.192	-0.316	-0.194	-0.317	-0.176	-0.477	-0.172	-0.478	-0.083	-0.543	-0.134	-0.588
4	-0.200	-0.303	-0.203	-0.305	-0.193	-0.456	-0.184	-0.463	-0.072	-0.492	-0.155	-0.554
5	-0.209	-0.287	-0.214	-0.290	-0.220	-0.425	-0.199	-0.444	-0.069	-0.442	-0.184	-0.514
6	-0.222	-0.268	-0.227	-0.271	-0.262	-0.377	-0.219	-0.421	-0.073	-0.394	-0.219	-0.468
7	-0.238	-0.246	-0.242	-0.250	-0.331	-0.305	-0.241	-0.395	-0.086	-0.347	-0.257	-0.416

TABLE V. Errors (experimental-theoretical, in cm^{-1}) in the energies of bound levels in the first excited bending state of Ne-CO. Results from the scaled version of the SAPT surface are shown in parentheses. The $J=0$, $K=0$, e level on S2 has energy -22.740 cm^{-1} ; $J=1$, $K=1$, f has energy -15.687 cm^{-1} .

J	$K=0,e$		$K=1,f$	
	SAPT	S2	SAPT	S2
0	0.328(0.066)	0.221		
1	0.323(0.063)	0.223	-0.510 (-0.7011)	-0.051
2	0.313(0.057)	0.225	-0.521 (-0.7101)	-0.047
3	0.299(0.048)	0.229	-0.538 (-0.7237)	-0.041
4	0.280(0.036)	0.234	-0.560 (-0.7421)	-0.032
5	0.258(0.023)	0.240	-0.587 (-0.7657)	-0.021
6	0.230(0.007)	0.248	-0.622 (-0.7950)	-0.006
7	0.199(-0.009)	0.256	-0.665 (-0.8306)	0.010

The values in Table IV increase as one moves down an S2 column, and decrease as one moves down a SAPT column. This pattern is consistent with the conclusion from the microwave results: The effective B rotational constant is too small on S2 and too large on the SAPT surface. For $K=0$, the microwave results showed that the SAPT model was clearly superior. For $K>0$, SAPT is still better but the difference is no longer so large. For example, for the e component of $K=2$, the B value fitted to the S2 results in Table IV is 0.0013 cm^{-1} lower than the corresponding experimental value while B from the SAPT results is 0.0009 cm^{-1} higher.

The SAPT surface predicts the origin of each K stack in the vibrational ground state with better accuracy than S2 does. Furthermore, the K origins predicted by S2 become steadily worse as K increases, while the error of the SAPT origins remains about the same. These origins do not follow a smooth pattern, as noted by McKellar and Chan, so it is difficult to make precise statements about errors in the S2 surface from them. It does appear, however, that the effective A constant (which corresponds roughly to rotation about the van der Waals bond) is too large on S2.

The scaled SAPT surface, whose errors are not shown in Table IV, predicts the origins of the $K=1$ stacks with about 0.02 cm^{-1} error and of the $K=2$ stacks with 0.14 cm^{-1} error. At $K=3$ its error in location of the f stack origin is 0.2 cm^{-1} , between those of the *ab initio* SAPT and S2 surfaces. In all the K stacks, the scaled surface gives a B constant that is larger (that is, less accurate) than the *ab initio* SAPT surface.

The results in Table V indicate that S2 gives a better description of the first bending vibration of Ne-CO. The experimental, S2, and SAPT fundamental frequencies are 8.5805 , 8.359 , and 8.253 cm^{-1} , respectively. Only one $K\neq 0$ stack is available for comparison, but it indicates that both surfaces give effective A constants in $v_2=1$ that are too large but the error on S2 is a factor of 3 or so smaller. The B constants from S2 are still smaller than experiment and those from SAPT are still larger, but now the S2 results are closer to experiment by roughly a factor of 2. (The excellent agreement of S2 with experiment in the last column of Table V is fortuitous; it arises from a cancellation of errors between an

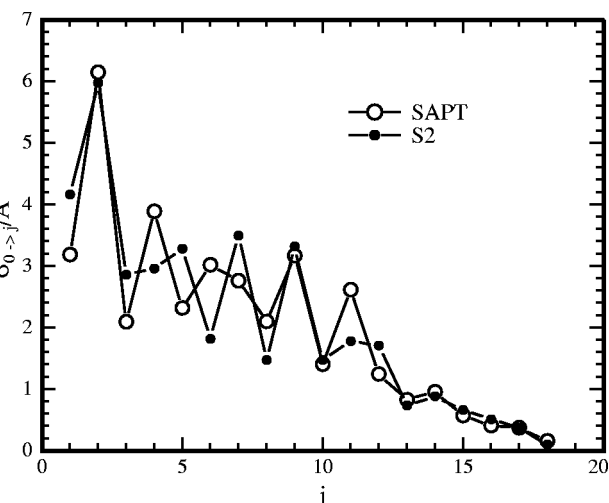


FIG. 3. $0 \rightarrow j$ integral cross sections at 711 cm^{-1} for the S2 and SAPT surfaces.

underestimated vibrational frequency and an overestimated A constant, and will not persist to other K stacks.)

Results from the scaled SAPT surface for the $v_2=1$ bending levels are shown in Table V in parentheses. For $K=0$, the scaling produces a much improved agreement with experiment; the errors in the energies are much smaller than those from either *ab initio* potential. The effective B constant is also improved in that K stack. The scaling does not improve agreement with the $K=1$ levels, however; in fact, they are worse in the scaled surface than in either of the *ab initio* surfaces. Most of the disagreement comes from a substantial overestimation of the A constant on the scaled surface. These observations are consistent with the discussion of McKellar and Chan.⁶

C. Integral cross sections

The accompanying experimental paper⁷ describes measurements of state-to-state integral cross sections for rotational excitation of CO by Ne and comparisons to the S2 and SAPT surfaces. The feature of the integral cross sections most sensitive to the potential surface is the interference structure that appears at low Δj . The S2 surface predicts the phase of the interference oscillations correctly, although it does not reproduce the amplitudes particularly well. The SAPT surface predicts the wrong phase at low Δj . It thus appears that the S2 surface is more accurate in the repulsive region.

In the comparison with experiment, averaging over initial rotational populations in the molecular beam and over the Ne isotope distribution effaces the predicted oscillations considerably. To demonstrate more clearly the differences and similarities in the two potentials' predictions, Fig. 3 shows the unaveraged $\sigma_{0 \rightarrow j}$ cross sections at 711 cm^{-1} predicted by the two surfaces. The overall decrease with Δj is very similar for the two potentials. On the other hand, the interference structure is quite different. Both show a maximum at $\Delta j=2$. The S2 cross sections then immediately switch phase, and show an odd Δj propensity up through $\Delta j=11$ before changing phase again. The SAPT cross sec-

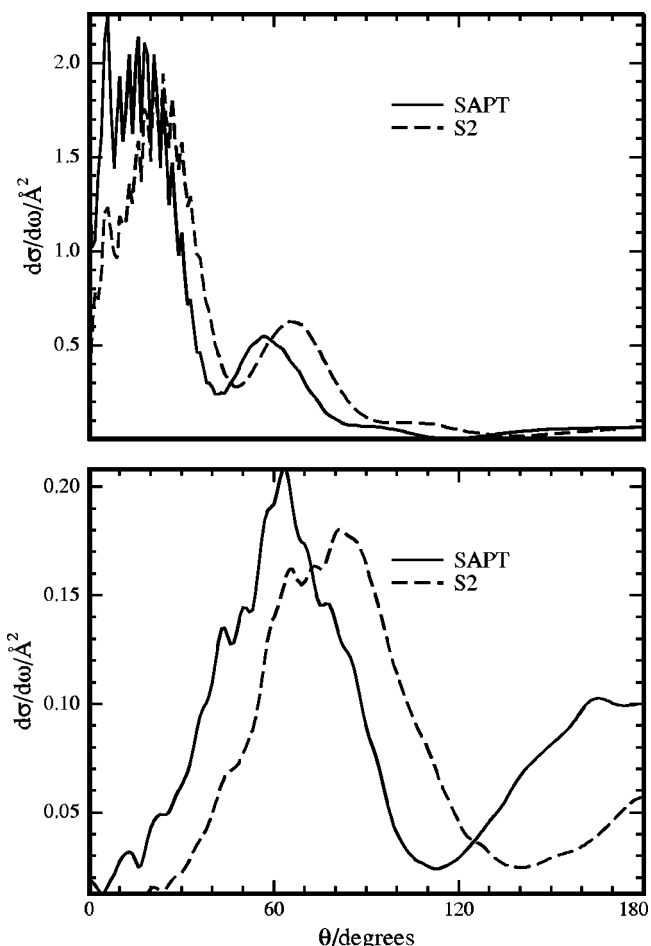


FIG. 4. $0 \rightarrow 5$ (upper panel) and $0 \rightarrow 12$ (lower panel) differential cross sections at 460 cm^{-1} for the SAPT and S2 surfaces.

tions, on the other hand, do not switch to odd Δj until $\Delta j = 8$. Unfortunately, it is difficult to relate these differences to specific features of the surfaces.

D. Differential cross sections

State-to-state differential cross sections are not yet available for Ne–CO rotationally inelastic scattering, although some experiments are under way.³² Figure 4 shows the predicted state-to-state differential cross sections at 460 cm^{-1} for the $0 \rightarrow 5$ and $0 \rightarrow 12$ collisional excitations for both surfaces. The cross sections were obtained with converged close-coupled (CC) calculations; the partial wave sum was terminated near $J = 113\hbar$.

The rotational rainbow maxima and minima appear at higher scattering angles in the S2 predictions, especially for the $0 \rightarrow 12$ transition. The difference probably reflects the slightly smaller anisotropy in the repulsive wall for the S2 surface; a more nearly head-on, and therefore higher scattering angle, transition is required to produce $\Delta j = 12$. The difference should be easily resolvable even in experiments of modest angular resolution. State-to-state DCS could therefore provide a much cleaner test of the accuracy of the two surfaces in the repulsive region than is currently available from the integral cross sections.

TABLE VI. Pressure broadening cross sections.

Temperature	Experiment (Ref. 33)	SAPT	S2
77 K	$64.5 \pm 7 \text{ Å}^2$	66.6	65.1
198 K	51 ± 6	49.8	49.3
294 K	42 ± 5	45.1	44.8

E. Pressure broadening

Nerf and Sonnenberg reported Ne pressure broadening cross sections in 1975³³ for the CO $1 \leftarrow 0$ rotational transition at 77, 198, and 294 K. At 77 K, $k_B T$ is roughly equal to the Ne–CO well depth, so the pressure broadening cross section is most sensitive to the attractive well and long-range parts of the potential. At the higher temperatures, the repulsive wall of the potential plays a more important role.

We evaluated pressure broadening cross sections with the MOLSCAT program²⁸ for both the SAPT surface and S2. Only the diagonal part of the cross section matrix was used; for the well-isolated $1 \leftarrow 0$ line and the modest pressures used in the experiment, the off-diagonal (intensity transfer) terms should not be important.³⁴

The temperature-dependent cross sections were obtained by thermal averages over cross sections computed at specific energies:

$$\sigma(T) = \left(\frac{1}{k_B T} \right)^2 \int_0^\infty \sigma(E) \exp(-E/k_B T) E dE. \quad (7)$$

For the numerical evaluation of $\sigma(T)$, the integral was broken into two sections, one at energies below 50 cm^{-1} and one at higher energy. The lower section was evaluated by straightforward trapezoidal rule integration with a 1 cm^{-1} energy grid. The cross sections at energies $E \leq 50 \text{ cm}^{-1}$ were obtained by close-coupled calculations. Some resonance structure appears in that region, but the resonances are not particularly sharp and the low energy section only contributes about one-third of the total cross section even at 77 K, so a much finer grid was not needed. The section above 50 cm^{-1} , where the cross sections are very smooth, was evaluated by four-point Gauss–Laguerre quadrature. Cross sections in that region were obtained by the coupled states approximation of McGuire and Kouri.²⁹ The total numerical error in the pressure broadening cross sections, resulting chiefly from the coarse integration grid and the use of CS calculations, probably does not exceed 3 Å^2 . The results are shown in Table VI. Both surfaces predict broadening cross sections well within the experimental error estimates.

F. Interaction second virial coefficients

Second virial coefficients for gas mixtures give information about the average “size” of the potential; they are sensitive the volume of the well at low temperatures, and to the hard core of the potential at high temperatures ($k_B T$ much greater than the well depth). Brewer³⁵ and Vatter *et al.*⁵ have reported interaction second virial coefficients for Ne–CO mixtures at several temperatures. Moszynski *et al.* computed the coefficients from the SAPT potential.³⁶ We have calcu-

TABLE VII. Interaction second virial coefficients. Data below 290 K are from Ref. 35, reproduced and assigned uncertainties in Ref. 36. Data above 290 K are from Ref. 5.

Temperature	Experiment	SAPT (Ref. 36)	S2
123.15 K	-14.7 ± 3.0 cm ³ /mol	-17.26	-14.48
148.15	-5.6 ± 3.0	-7.50	-5.28
173.15	-0.42 ± 3.0	-0.96	0.90
223.15	7.83 ± 2.0	7.15	8.57
273.15	12.23 ± 2.0	11.88	13.04
296.15	14.1 ± 1.5	13.43	14.35
353.15	17.2 ± 2.0	16.24	17.03
463.15	20.6 ± 3.0	19.34	19.97

lated the coefficients from S2 using the expressions given by Pack.³⁷ Table VII lists our results and the experimental data, and also includes values for the SAPT potential for completeness. All the first order quantum corrections have been included. The quantum corrections contribute 0.7 cm³/mol at the lowest temperature, and about ten times less at the highest temperature.

The virial coefficients computed from the SAPT potential are lower than those computed from S2 at all temperatures. The consistent difference reflects the deeper well and slightly smaller repulsive core of the SAPT potential. The two potentials' predictions are all within the experimental error bars. Experimental accuracy on the order of 1 cm³/mol, not quite realizable with the best current techniques, would be required to cleanly select one of the two potentials over the other.

V. DISCUSSION

Our original hope was that a high quality supermolecule surface would give a better description of the repulsive wall of the Ne–CO interaction. S2 does give improved, although still not quantitative, agreement with the interference oscillations in the rotational excitation cross sections. This comparison provides modest evidence that the shape of the S2 repulsive wall is more realistic than that of the SAPT surface. State-to-state differential cross sections, when they become available, will provide a more incisive comparison between the models and may also suggest specific deficiencies in the surfaces.

The *ab initio* SAPT surface provides the best current description of the ground state of NeCO. The microwave data suggest that its $\langle R \rangle$ is very slightly too short but is probably within 0.01 Å of the correct value. No other available surface matches this accuracy.

For the first excited vibrational state of NeCO, whose wave function occupies a wider region of the attractive well, the limited IR data suggest that S2 is more realistic. However, since the SAPT surface appears to have a more realistic minimum, SAPT may be a better model for predicting energies of levels with excitations in the van der Waals stretch.

The errors in S2 have three origins: finite basis set size, incomplete treatment of electron correlation, and fitting errors. Fitting errors are probably the least important in the comparisons to experiment we have presented here; several

different fitting procedures produced nearly identical experimental predictions. The most important contributor to errors on the surface may be basis set size. We developed two different potential energy surfaces using basis sets which differed by only two functions. For some properties we evaluated, the differences were significant, and in every case the larger basis set produced the more accurate result. This provides some hope that the basis sets we used are approaching saturation. Comparison of the results of the single point calculations described earlier, at $R=3.4$ Å and $\Theta=80^\circ$, with the aug-cc-pVDZ+(3s3p2d), aug-cc-pVTZ+(3s3p2d), and aug-cc-pVQZ+(3s3p2d) basis sets also suggests that further increases in basis set size will provide a smooth increase in accuracy.

Both of the experiments that S2 fits better—the scattering and hot-band IR data—involve relatively close approach of the Ne atom to the CO, where intramonomer electron correlation is important to evaluation of exchange-repulsion energies. The treatment of intramonomer correlation effects in the supermolecule CCSD(T) approach is more sophisticated than in the perturbation approach of Moszynski *et al.*¹ which, depending on the energy component, uses various methods that range from MP2 to CCSD. The relative success of S2 in those experiments could be caused by the better treatment of correlation, basis set effects on the perturbation theory monomer wave functions, or the truncation of the perturbation expansion after the second order in the interaction.

ACKNOWLEDGMENTS

The authors thank R. Moszynski and A. van der Avoird for providing their surfaces and for useful discussions, and the Ohio Supercomputer Center for many CPU cycles. S.M.C. acknowledges the support of National Science Foundation (Grant No. CHE-9616683).

- ¹R. Moszynski, T. Korona, P. E. S. Wormer, and A. van der Avoird, *J. Phys. Chem. A* **101**, 4690 (1997).
- ²R. W. Randall, A. J. Cliffe, B. J. Howard, and A. R. W. McKellar, *Mol. Phys.* **79**, 1113 (1993).
- ³J. Kestin, S. T. Ro, and W. A. Wakeham, *Ber. Bunsenges. Phys. Chem.* **86**, 753 (1982).
- ⁴R. D. Trengrove, H. L. Robjohns, and P. J. Dunlop, *Ber. Bunsenges. Phys. Chem.* **88**, 450 (1984).
- ⁵K. Vatter, H. J. Schmidt, E. Elias, and B. Schramm, *Ber. Bunsenges. Phys. Chem.* **100**, 73 (1996).
- ⁶A. R. W. McKellar and M. C. Chan, *Mol. Phys.* **93**, 253 (1998).
- ⁷S. Antonova, A. P. Tsakotellis, A. Lin, and G. C. McBane, *J. Chem. Phys.* **110**, 11742 (1999), following paper.
- ⁸G. Chalasiński and M. M. Szczęśniak, *Chem. Rev.* **94**, 1723 (1994).
- ⁹D. E. Woon, K. A. Peterson, and T. H. Dunning Jr., *J. Chem. Phys.* **109**, 2233 (1998).
- ¹⁰T. van Mourik and T. H. Dunning Jr., *J. Chem. Phys.* **107**, 2451 (1997).
- ¹¹K. Raghavachari, G. W. Trucks, J. A. Pople, and M. Head-Gordon, *Chem. Phys. Lett.* **157**, 479 (1989).
- ¹²T. H. Dunning Jr., *J. Chem. Phys.* **90**, 1007 (1989).
- ¹³R. A. Kendall, T. H. Dunning Jr., and R. J. Harrison, *J. Chem. Phys.* **96**, 6796 (1992).
- ¹⁴D. E. Woon and T. H. Dunning Jr., *J. Chem. Phys.* **100**, 2975 (1994).
- ¹⁵F.-M. Tao and Y.-K. Pan, *J. Chem. Phys.* **97**, 4989 (1992).
- ¹⁶H. Koch, B. Fernandez, and O. Christiansen, *J. Chem. Phys.* **108**, 2784 (1998).
- ¹⁷S. F. Boys and F. Bernardi, *Mol. Phys.* **19**, 553 (1970).

- ¹⁸C. Hampel, K. A. Peterson, and H.-J. Werner, *Chem. Phys. Lett.* **190**, 1 (1992).
- ¹⁹M. J. O. Deegan and P. J. Knowles, *Chem. Phys. Lett.* **227**, 321 (1994).
- ²⁰MOLPRO is a package of *ab initio* programs written by H.-J. Werner and P. J. Knowles with contributions from J. Almlöf, R. D. Amos, A. Berning, M. J. O. Deegan, F. Eckert, S. T. Elbert, C. Hampel, R. Lindh, W. Meyer, A. Nicklass, K. Peterson, R. Pitzer, A. J. Stone, P. R. Taylor, M. E. Mura, P. Pulay, M. Schuetz, H. Stoll, T. Thorsteinsson, and D. L. Cooper.
- ²¹R. Bukowski, J. Sadlej, B. Jeziorski, P. Jankowski, K. Szalewicz, S. A. Kucharski, H. L. Williams, and B. M. Rice, *J. Chem. Phys.* **110**, 3785 (1999).
- ²²R. A. Kendall, G. Chałasiński, J. Kłos, R. Bukowski, M. W. Severson, M. M. Szczęśniak, and S. M. Cybulski, *J. Chem. Phys.* **108**, 3235 (1998).
- ²³S. M. Cybulski, J. Couvillion, J. Kłos, and G. Chałasiński, *J. Chem. Phys.* **110**, 1416 (1999).
- ²⁴K. T. Tang and J. P. Toennies, *J. Chem. Phys.* **80**, 3726 (1984).
- ²⁵J. M. Hutson, *Comput. Phys. Commun.* **84**, 1 (1994).
- ²⁶J. M. Hutson, BOUND computer code, version 5 (1993), distributed by Collaborative Computational Project No. 6 of the Science and Engineering Research Council (U.K.).
- ²⁷D. E. Manolopoulos, *J. Chem. Phys.* **85**, 6425 (1986).
- ²⁸J. M. Hutson and S. Green, MOLSCAT computer code, version 14 (1994), distributed by Collaborative Computational Project No. 6 of the Engineering and Physical Sciences Research Council (U.K.).
- ²⁹P. McGuire and D. J. Kouri, *J. Chem. Phys.* **60**, 2488 (1974).
- ³⁰M. H. Alexander and D. E. Manolopoulos, *J. Chem. Phys.* **86**, 2044 (1987).
- ³¹K. A. Walker, T. Ogata, W. Jäger, M. C. L. Gerry, and I. Ozier, *J. Chem. Phys.* **106**, 7519 (1997).
- ³²K. T. Lorenz and D. W. Chandler, private communication.
- ³³R. B. Nerf, Jr. and M. A. Sonnenberg, *J. Mol. Spectrosc.* **58**, 474 (1975).
- ³⁴M. Thachuk, C. E. Chuaqui, and R. J. Le Roy, *J. Chem. Phys.* **105**, 4005 (1996).
- ³⁵J. Brewer, AFOSR Technical Report MRL-2915-C, 1967, cited in Ref. 36.
- ³⁶R. Moszynski, T. Korona, T. G. A. Heijmen, P. E. S. Wormer, A. van der Avoird, and B. Schramm, *Pol. J. Chem.* **72**, 1479 (1998).
- ³⁷R. T Pack, *J. Chem. Phys.* **78**, 7217 (1983).